

FEM-Based A-Optimal Sensor Placement for Heat Source Inversion From Final Time Measurement

Christian Aarset^[0000-0001-8163-9305],
Tram Thi Ngoc Nguyen^[0000-0002-7245-7611]

1 Experimental design for heat source identification

This article concerns itself with optimal experimental design (OED) for reconstruction in the inverse heat source problem. The heat equation models heat dispersal over time from a heat source through a spatial domain by solving a time-dependent partial differential equation (PDE). Inverting the heat equation serves to reconstruct and identify the unknown heat source, of great interest in controlling and optimizing heating and cooling processes for various applications, e.g. in materials science.

A natural question arises: what is the optimal configuration of sensors, or *optimal design* for data collection, yielding the best possible reconstruction of the unknown heat source? We assume that in the spatial domain, a total of m different fixed candidate locations are proposed for sensor placement, while due to budget constraints, one can place no more than $m_0 < m$ of all potential sensors. One strategy would be to repeat the experiment $\binom{m}{m_0}$ times and choose the sensor configuration that yielded the best reconstruction in practice. However, this quickly becomes unfeasible for even modest values of m and m_0 , due to combinatorial scaling; moreover, it is desirable to fix the design a priori, avoiding the need for a test-trial phase for data collection.

We assume that each sensor provides only a single scalar observation of the (local approximation to the) heat at its placement location at a fixed final measurement time $T > 0$. In what follows, we present an adaptation of the low-rank approximation-based *redundant-dominant p-continuation algorithm* recently invented by one of the authors in [1] to obtain A-optimal designs, that is, sensor placements that minimise the trace of the posterior covariance, equivalently, that minimise average posterior

Christian Aarset
University of Göttingen - Institute for Numerical and Applied Mathematics, Lotzestr. 16-18, D-37083 Göttingen, Germany, e-mail: c.aarset@math.uni-goettingen.de

Tram Thi Ngoc Nguyen
Max Planck Institute for Solar Systems Research, Justus-von-Liebig-Weg 3, 37077 Göttingen, Germany, e-mail: nguyen@mps.mpg.de

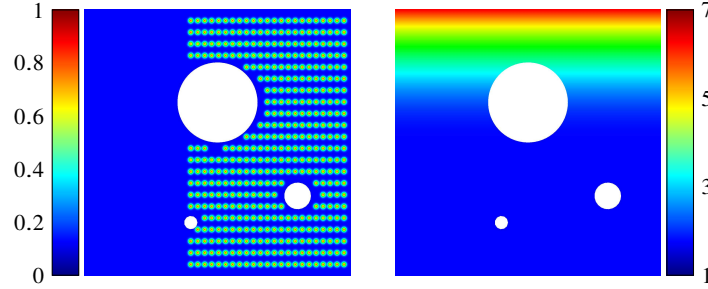


Fig. 1 Left: Source domain, full domain and grid of all candidate sensor locations. Right: Spatially dependent diffusion parameter α in (6).

pointwise uncertainty in the reconstruction, see Section 2. For a deeper discussion of this and related topics, we refer to [2].

In so doing, we demonstrate the applicability of the results in [1] to time-dependent PDEs, showcasing its relevance to a broad class of problems. Several key elements must be taken into account: well-posedness of the forward heat model, efficiency of the backpropagator and the adaptation of the finite element method (FEM) framework to the time-dependent PDE. These aspects, and their introduction to the A-optimal computational framework, form the contribution of this article.

Notation. Finite-dimensional vectors are denoted by boldface lowercase letters (i.e. \mathbf{g} , \mathbf{w}), scalars and function space variables are denoted by plainface lowercase letters (e.g. p , s), matrices are denoted by plainface uppercase letters (e.g. F , Γ), while operators with infinite-dimensional inputs or outputs employ calligraphic uppercase letters (e.g. \mathcal{S} , \mathcal{O}). For any vector space X , the (topological) dual space is X^* .

2 A-optimal sensor placement

Design-dependent forward map. The *sensor placement problem* is to find the experimental design $\mathbf{w} \in \{0, 1\}^m$, $m \in \mathbb{N}$, allowing for the best reconstruction of a source s in some Hilbert space X , given the design-dependent forward map

$$\mathcal{F}_{\mathbf{w}} : X \rightarrow \mathbb{R}^m, \quad \mathcal{F}_{\mathbf{w}} := \text{Diag}(\mathbf{w})\mathcal{F}, \quad \mathcal{F} : X \rightarrow \mathbb{R}^m, \quad (1)$$

where $\text{Diag}(\mathbf{w}) : \mathbb{R}^m \rightarrow \mathbb{R}^m$ is the multiplication operator, represented as a diagonal matrix. As $\mathbf{w} \in \{0, 1\}^m$, the design \mathbf{w} acts as a mask on the data, representing the act of sensor placement. The quantity m thus represents the number of candidate locations where the experimenter might elect to place a sensor.

A-optimality. For Bayesian linear inverse problems, an *A-optimal design* can be expressed as the minimiser of the trace of the posterior covariance. Recall from [3, 14] that if the unknown s has Gaussian prior $\mathcal{N}(s_0, C_0)$, $s_0 \in X$, $C_0 : X^* \rightarrow X$ and the measurement is corrupted by additive Gaussian noise $\epsilon \sim \mathcal{N}(0, \Gamma)$ in \mathbb{R}^m , where

$\Gamma \in \mathbb{R}^{m \times m}$ is diagonal and positive definite, then for each design \mathbf{w} , the posterior distribution of s given observed noisy data $\mathbf{g} \in \mathbb{R}^m$ is $s|\mathbf{g} \sim \mathcal{N}(s_{\text{post}}(\mathbf{w}), C_{\text{post}}(\mathbf{w}))$,

$$s_{\text{post}}(\mathbf{w}) := s_0 + C_{\text{post}}(\mathbf{w}) \mathcal{F}_{\mathbf{w}}^* \Gamma^{-1} (\mathbf{g} - \mathcal{F}_{\mathbf{w}} s_0), \quad (2)$$

$$C_{\text{post}}(\mathbf{w}) := \left(\mathcal{F}_{\mathbf{w}}^* \Gamma^{-1/2} \text{Diag}(\mathbf{w}) \Gamma^{-1/2} \mathcal{F}_{\mathbf{w}} + C_0^{-1} \right)^{-1}. \quad (3)$$

The A-optimal objective thus becomes

$$\mathcal{J} : \mathbf{w} \in \mathbb{R}^m \mapsto \text{tr}(C_{\text{post}}(\mathbf{w})) = \text{tr} \left(\left(\mathcal{F}_{\mathbf{w}}^* \Gamma^{-1/2} \text{Diag}(\mathbf{w}) \Gamma^{-1/2} \mathcal{F}_{\mathbf{w}} + C_0^{-1} \right)^{-1} \right); \quad (4)$$

which is well-defined for all non-negative \mathbf{w} . A (p -relaxed) A-optimal design \mathbf{w}^{*p, m_0} , $p \in [0, 1]$ using no more than m_0 sensors then satisfies

$$\mathbf{w}^{*p, m_0} \in \underset{\mathbf{w} \in [0, 1]^m, \|\mathbf{w}\|_p \leq m_0}{\text{argmin}} \mathcal{J}(\mathbf{w}). \quad (5)$$

[1, Thm. 8] guarantees that $\mathbf{w}^{*0, m_0} \in \{0, 1\}^m$, i.e. it is *binary*, while the optimisation is convex and solvable for $p = 1$, although \mathbf{w}^{*1, m_0} is generally only partially binary.

3 Heat model and the forward map

Linear heat equation. Consider the room $\Omega := (-1, 1)^2$ with boundary $\partial\Omega = B_{\text{int}} \cup B_{\text{ext}}$, where both the surfaces B_{int} of the rods permeating the domain and the exterior boundaries B_{ext} are thermally insulated, which we model via homogeneous Neumann boundary conditions. The heat distribution $u \in \mathcal{U}$ in the room from a spatially dependent heat source s is governed by the linear parabolic equation

$$\begin{cases} \dot{u} - \nabla \cdot (a \nabla u) = s & \text{in } \Omega \times (0, T), \\ \partial_{\mathbf{n}} u = 0 & \text{on } \partial\Omega \times [0, T], \\ u(t = 0) = 0 & \text{on } \Omega, \end{cases} \quad (6)$$

where the source $s \in X := L^2(\Omega_S)$ is implicitly extended by zero outside its *source domain* $\Omega_S := (-1, -0.5) \times (-1, 1)$. Here, \dot{u} denotes the time derivative, the diffusion parameter is $a(\mathbf{x}) = 1 + (5x_2^5 + x_2^3) \chi_{x_2 \geq 0} \in C(\bar{\Omega})$, see Figure 1, and \mathbf{n} indicates the outward normal vectors at the boundaries. The PDE (6) is well-posed in the sense that for any source $s \in X$, there exists a unique weak solution to (6) with

$$u \in \mathcal{U} := L^2(0, T; H^1(\Omega)) \cap H^1(0, T; H^1(\Omega)^*), \quad \|u\|_{\mathcal{U}} \leq C \|s\|_X \quad (7)$$

for some constant C (cf. [5, 8]). We thus define the linear source-to-final-state map

$$\mathcal{S} : X \rightarrow L^2(\Omega), \quad s \mapsto u(\cdot, T) \quad (8)$$

which is well defined due to the continuous embedding $\mathcal{U} \hookrightarrow C(0, T; L^2(\Omega))$, as well as injective [7].

Finite measurement. A central conceit of sensor placement is that the state can only be measured as a possibly rather small vector of observables. This requires composition with the *finite measurement operator* $\mathcal{O} : L^2(\Omega) \rightarrow \mathbb{R}^m$, given as

$$\mathcal{O}u := \left((o_k, u)_{L^2(\Omega)} \right)_{k=1}^m \in \mathbb{R}^m$$

for all $u \in L^2(\Omega)$. The functions $(o_k)_{k=1}^m \subset L^2(\Omega)$ can be thought of as *sensors* [1]. This formulation finally leads us to the *source-to-observable* map $\mathcal{F} : X \rightarrow \mathbb{R}^m$,

$$\mathcal{F}s := [\mathcal{O} \circ \mathcal{S}]s = \left((o_k, \mathcal{S}s)_{L^2(\Omega)} \right)_{k=1}^m \in \mathbb{R}^m \quad \text{for all } s \in X.$$

4 FEM-based A-optimality via the RedDom- p algorithm

The *redundant-dominant p -continuation algorithm* introduced by one of the authors in [1] stands as a robust, high-performing algorithm for sensor placement. Leveraging global optimality theory [1, Thm. 3] to mark sensors as *dominant* and *redundant*, i.e. always on or off, it enables significant dimensionality reduction of the OED.

Algorithm 1 Binary OED by p -continuation via redundant-dominant classification

Input: Initialisation as globally optimal non-binary design $\mathbf{w}^0 := \mathbf{w}^{*1, m_0}$ from (5), power $p = 1$, iteration $i = 0$, continuation parameter $\delta \in (0, 1)$

- 1: **while** \mathbf{w}^i has entries significantly different from 0 and 1 **do**
- 2: $p \leftarrow (1 - \delta)p$ and $i \leftarrow i + 1$
- 3: Solve the non-convex constrained optimization problem (e.g. via the SLSQP algorithm)

$$\mathcal{J}^p(\mathbf{z}) := \mathcal{J}(\mathbf{z}^{1/p}), \quad (9)$$

$$\nabla \mathcal{J}^p(\mathbf{z}) = \frac{1}{p} \nabla \mathcal{J}(\mathbf{z}^{1/p}) \mathbf{z}^{1/p-1}, \quad (10)$$

$$0 \leq z_k \leq 1 \quad \text{for all } k \in \mathbb{N}, k \leq m, \quad \sum_{k=1}^m z_k \leq m_0, \quad (11)$$

initialised at $\mathbf{z} := (\mathbf{w}^{i-1})^p$ and keeping dominant and redundant indices ($w_k^{*1, m_0} = 1$, resp. $w_k^{*1, m_0} = 0$) fixed, returning \mathbf{z}^i

- 4: $\mathbf{w}^i \leftarrow (\mathbf{z}^i)^{1/p}$

5: **end while**

Output: Binary design $\bar{\mathbf{w}}^{m_0} := \mathbf{w}^i$ as approximate binary optimal design.

This algorithm requires the adjoint of the source-to-observable map \mathcal{F} :

Lemma 1 (Backpropagator) *The adjoint $\mathcal{F}^* : \mathbb{R}^m \rightarrow L^2(\Omega_S)$ is given by*

$$\mathcal{F}^* \mathbf{g} = \int_0^T R_0 z dt \quad \text{where} \quad \begin{cases} -\dot{z} - \nabla \cdot (a \nabla z) = 0 & \text{in } \Omega \times (0, T), \\ \partial_n z = 0 & \text{on } \partial\Omega \times [0, T], \\ z(t = T) = \sum_{k=1}^m g_k o_k & \text{on } \Omega, \end{cases} \quad (12)$$

with $R_0 : L^2(\Omega) \rightarrow L^2(\Omega_S)$ being the restriction operator.

Proof. The restriction R_0 is clearly well-defined. With $s \in L^2(\Omega_S)$, $\mathbf{g} \in \mathbb{R}^m$, write $u(T) := \mathcal{S}s \in L^2(\Omega)$, implying $\dot{u} - \nabla \cdot (a \nabla u) = s$ in $\Omega_S \times (0, T)$ and 0 elsewhere. We write the inner product via partial integrations in Bochner spaces, that is

$$\begin{aligned} (\mathcal{F}s, \mathbf{g})_{\mathbb{R}^m} &= \sum_{k=1}^m (o_k, \mathcal{S}s)_{L^2(\Omega)} g_k = \sum_{k=1}^m \int_{\Omega} u(T) g_k o_k dx \\ &= \int_{\Omega} u(T) \left(\sum_{k=1}^m g_k o_k \right) dx + \int_0^T \int_{\Omega} u (-\dot{z} - \nabla \cdot (a \nabla z)) dx dt \\ &= \int_{\Omega} u(T) \left(\left(\sum_{k=1}^m g_k o_k \right) - z(T) \right) dx + \int_{\Omega} u(0) z(0) dx \\ &\quad + \int_0^T \int_{\Omega} (\dot{u} - \nabla \cdot (a \nabla u)) z dx dt \\ &= 0 + 0 + \left(\int_0^T z dt, s \right)_{L^2(\Omega_S)} \end{aligned}$$

where z solves the adjoint equation (12), as s is independent of time and is supported on Ω_S . Above, we make use of homogeneous boundary conditions of u, z and the Bochner integral identity [13, Lemma 7.3]: $(u(T), z(T))_{L^2(\Omega)} - (u(0), z(0))_{L^2(\Omega)} = \int_0^T \langle \dot{u}(t), z(t) \rangle_{H^1(\Omega)^*, H^1(\Omega)} - \langle u(t), \dot{z}(t) \rangle_{H^1(\Omega), H^1(\Omega)^*} dt$ for $u, z \in \mathcal{U}$. \square

5 Numerical results

To obtain our numerical results, we take a FEM discretisation of $L^2(\Omega)$ as a second-order finite element space with $n_{\text{co}} := 17727$ degrees of freedom, containing $X = L^2(\Omega_S) \subset L^2(\Omega)$ as a subset with $n := 5289$ associated degrees of freedom. We obtain FEM discretisations of the forward and adjoint maps $\mathcal{F}, \mathcal{F}^*$ via the NGSOLVE software's NGSXFEM integration and the associated time-space finite element spaces, taking time-steps of $\Delta t = 10^{-4}$ over the time interval $[0, 1]$.

While forward resp. adjoint evaluations \mathcal{F} resp. \mathcal{F}^* solve time-dependent PDEs, they can both be viewed as mappings between finite element coefficients and vector observables. Thus, we replace them by their respective halves of the prior-preconditioned misfit Hessian, writing $F := \Gamma^{-1/2} \mathcal{F} C_0^{1/2} \mathbf{M}^{1/2} \in \mathbb{R}^{m \times n}$, $F^T = \mathbf{M}^{-1/2} C_0^{1/2} \mathcal{F}^* \Gamma^{-1/2}$. The half-powers of the mass matrix \mathbf{M} act as isometric

isomorphisms between the finite element discretisation of X and standard Euclidean space, see [1]. We obtained low-rank decompositions $F^T \approx QR$ and $F \approx R^T Q^T$, with $Q \in \mathbb{R}^{n \times \ell}$, $R \in \mathbb{R}^{\ell \times m}$, $\ell = 50 \ll \min\{m, n\}$ by repeated forward-adjoint evaluations with the randomised subspace iteration algorithm [6]. ℓ was chosen automatically, with a ratio of 10^{-12} between largest and smallest approximate singular values of F . As time-integration in the adjoint computation \mathcal{F}^* via (12) must be done via numerical integration, and the randomised subspace iteration algorithm is sensitive to numerical accuracy of the adjoint, the value Δt must be chosen low. However, once the low-rank decomposition has been computed, this incurs no further cost, as the low-rank form maps directly from source coefficients to final-time measurements without intermediate-time calculations.

Lemma 2 (Algorithm 1 – Low-rank) *The low-rank approximations of the objective (9) and gradient (10) in Algorithm 1 for A-optimal design (4) take the form*

$$\mathcal{J}(\mathbf{w}) = \text{tr}(C_0) - \text{tr}(C) + \text{tr}\left(\left(R \text{Diag}(\mathbf{w})R^T + I_\ell\right)^{-1} C\right), \quad (13)$$

$$\nabla \mathcal{J}(\mathbf{w}) = -\text{ColumnNorm}\left(C^{1/2}\left(R \text{Diag}(\mathbf{w})R^T + I_\ell\right)^{-1} R\right), \quad (14)$$

where $C := Q^T \mathbf{M}^{1/2} C_0 \mathbf{M}^{-1/2} Q \in \mathbb{R}^{\ell \times \ell}$ and ColumnNorm maps a (finite-dimensional) matrix to the vector containing the norms of each of its columns.

Proof. We refer to [1, Theorem 8]. □

As prior for Bayesian inversion, we choose $f \sim \mathcal{N}(0, C_0)$, where $C_0 := (-\alpha\Delta + I)^{-2}$ is the densely defined bounded linear inverse bilaplacian operator on $L^2(\Omega_S)$, endowed with the Robin boundary condition $\frac{\partial}{\partial n} u = \frac{\sqrt{\alpha}}{1.42} u$, $\alpha = 1/4$. This prior is chosen as a moderately smoothing, trace class prior, whose boundary condition is known to lead to spatially uniform prior variance [4]. Noise on the finite measurement was realised as 1% of the average variance of one thousand data samples $(\mathcal{F} s^i)_{i=1}^n$, with each s^i drawn from the prior distribution, echoing the strategy employed in [1]. Our low-rank Algorithm 1 with Lemma 2 delivers the sequence $(\bar{\mathbf{w}}^{m_0})_{m_0=1}^{36} \subset \{0, 1\}^m$ of binary approximate A-optimal designs. The left side of Figure 2 visualises the optimal designs versus the *posterior pointwise variance field* $c : \Omega \rightarrow \mathbb{R}$, $c(\mathbf{x}) := [C_{\text{post}}(\mathbf{w})\delta_{\mathbf{x}}](\mathbf{x})$; this is an excellent visualisation of the uncertainty reduction by the design due to the relationship $\text{tr}(C_{\text{post}}(\mathbf{w})) = \int_{\Omega} c(\mathbf{x}) \, d\mathbf{x}$ [9].

The right side of Figure 2 compares A-optimality of $(\bar{\mathbf{w}}^{m_0})_{m_0=1}^{36}$ to random designs: For each m_0 , 10^3 random designs were drawn, their A-optimality plotted in red. To study one of the designs in depth, fix $m_0 = 36$. The artificial heat source s is $s(\mathbf{x}) := \exp(-1/r_{\pm}(\mathbf{x})^{1/8})$ whenever $r_{\pm}(\mathbf{x}) := (\frac{3\pi}{40})^2 - (x_1 + 0.75)^2 - (x_2 \pm 0.7)^2 > 0$ and 0 otherwise. Figure 3 shows the maximum a posteriori estimates of s with our proposed approximate optimal design $\mathbf{w} := \bar{\mathbf{w}}^{m_0}$ (left) and the best random design $\mathbf{w} := \mathbf{w}_{\text{RNG}}^{m_0}$ (right). Relative reconstruction errors are $\|s - s_{\bar{\mathbf{w}}^{m_0}}\|_2 / \|s\| \approx 0.6491$ and $\|s - s_{\mathbf{w}_{\text{RNG}}^{m_0}}\|_2 / \|s\| \approx 0.6782$. While both errors are large due to the limited

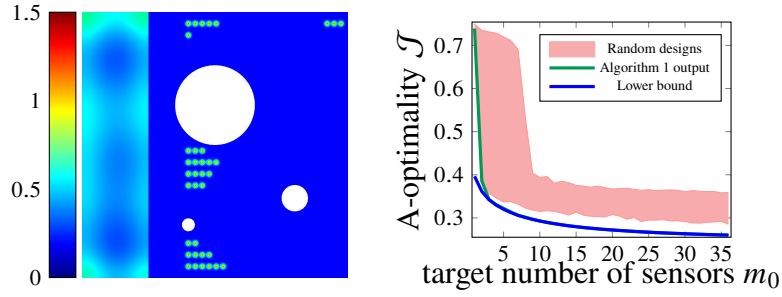


Fig. 2 Left: Optimal experimental design for $m_0 = 36$, with corresponding pointwise variance field. Colourbar max matches max of prior pointwise variance field $c_0(\mathbf{x}) := [C_0 \delta_{\mathbf{x}}](\mathbf{x})$. Right: Theoretical lower bound for A-optimality $\mathcal{J}(\mathbf{w}^{*1,m_0})$ (blue) via (5) [1, Thm. 3], proposed binary A-optimal designs $\bar{\mathbf{w}}^{m_0}$ (green, overlapping blue) and 10^3 random designs (red).

measurement data, the reconstructions are qualitatively good; our proposed solution attains 4.3% lower relative error than the random design.

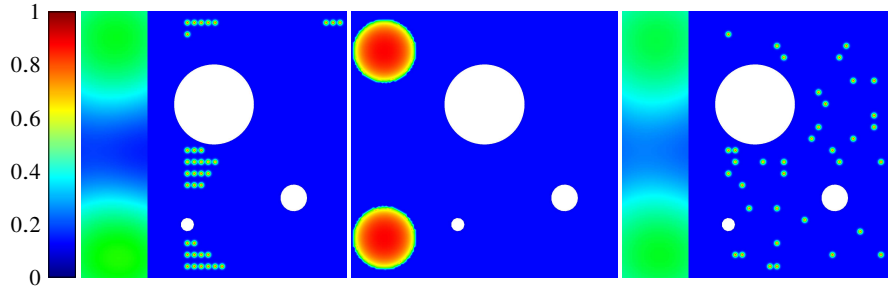


Fig. 3 Left: Maximum a posteriori estimate $s_{\bar{\mathbf{w}}^{m_0}}$ with proposed design. Center: True s . Right: Maximum a posteriori estimate $s_{\mathbf{w}_{\text{RNG}}^{m_0}}$ with random design.

6 Conclusions

In this work, we have demonstrated that the low-rank-based redundant-dominant p -continuation algorithm can be applied to obtain binary A-optimal designs for time-dependent PDE-based inverse problems, producing high-quality designs in low time. This suggests the validity of the method proposed in [1] to a broad class of physically relevant equations, significantly widening its scope. However, it is also clear that more informative data is required to obtain good reconstructions with only a small number of sensor placements; as such, the authors next intend to consider

also scenarios where multiple measurements are made in each sensor over different time points, in accordance to the setting of [1, Thm. 17], particularly in the context of e.g. trace data. To further accelerate the process of identifying optimal designs, the authors moreover plan on applying a bi-level [11, 12] or all-at-once [10] formulation to obtain further gains in terms of computational speed and robustness.

Acknowledgements The authors acknowledge support from the DFG through Grant 432680300 - SFB 1456 (C04).

References

1. Aarset, C.: Global optimality conditions for sensor placement, with extensions to binary a-optimal experimental designs. *Inverse Probl.* **41**(6), 065013 (2024)
2. Alexanderian, A.: Optimal experimental design for infinite-dimensional Bayesian inverse problems governed by pdes: a review. *Inverse Probl.* **37**(4), 043001 (2021)
3. Attia, A., Constantinescu, E.: Optimal experimental design for inverse problems in the presence of observation correlations. *SIAM J. Sci. Comput.* **44**(4), A2808–A2842 (2022)
4. Daon, Y., Stadler, G.: Mitigating the influence of the boundary on PDE-based covariance operators. *Inverse Probl. Imaging* **12**, 1083–1102 (2018)
5. Evans, L.C.: *Partial Differential Equations*, *Grad. Stud. Math.*, vol. 19. Am. Math. Soc., Providence, RI (1998)
6. Halko, N., Martinsson, P.G., Tropp, J.A.: Finding structure with randomness: probabilistic algorithms for constructing approximate matrix decompositions. *SIAM Rev.* **53**(2), 217–288 (2011)
7. Isakov, V.: *Inverse Source Problems*. Am. Math. Soc., Providence, RI (1990)
8. Kaltenbacher, B., Nguyen, T.T.N., Scherzer, O.: The tangential cone condition for some coefficient identification model problems in parabolic PDEs. In: *Time-Depend. Probl. Imaging Param. Identif.*, pp. 121–163. Springer, Cham (2021)
9. Mercer, J., Forsyth, A.R.: Functions of positive and negative type, and their connection with the theory of integral equations. *Philos. Trans. R. Soc. Lond. Ser. A* **209**(441–458), 415–446 (1909)
10. Nguyen, T.T.N.: Landweber–Kaczmarz for parameter identification in time-dependent inverse problems: all-at-once versus reduced version. *Inverse Probl.* **35**(3), 035009 (2019)
11. Nguyen, T.T.N.: Bi-level iterative regularization for inverse problems in nonlinear PDEs. *Inverse Probl.* **40**(4), 36 (2024)
12. Nguyen, T.T.N.: Sequential bi-level regularized inversion with application to hidden reaction law discovery. *Inverse Probl.* **41**(6), 34 (2025)
13. Roubíček, T.: *Nonlinear Partial Differential Equations with Applications*. Springer, Basel (2013)
14. Stuart, A.: Inverse problems: a Bayesian perspective. *Acta Numer.* **19**, 451–559 (2010)